

Excitation and Structure Change of ^{24}Mg . I— *Triaxial Deformed Mean Field in Low-Lying States* —Masaaki KIMURA,¹ Ryosuke YOSHIDA² and Masahiro ISAKA²¹*Creative Research Institution (CRIS), Hokkaido University,
Sapporo 001-0021, Japan*²*Department of Physics, Hokkaido University, Sapporo 060-0810, Japan*

(Received September 14, 2011; Revised January 6, 2012)

By using the antisymmetrized molecular dynamics with Gogny effective interaction, the low-lying spectrum and the $E2$ transition rates of ^{24}Mg are studied. On the basis of the comparison of the spectrum with observations, the importance of γ deformation in both positive- and negative-parity states is emphasized. Among the seven bands obtained, $K^\pi = 2^+$, 0^- and 3^- bands are triaxial deformed, and the inclusion of the degree of freedom of γ deformation is found to be essential to describe them.

Subject Index: 211, 212, 213

§1. Introduction

The recent development of nuclear structure models has enabled us theoretical investigation of a rich variety of structure and dynamics in nuclear many-body systems, which manifest up to highly excited states without *a priori* assumption. For example, in the case of *sd*-shell nuclei, various deformed states and (large-amplitude) collective excitations in the low-lying states are discussed on the basis of the generator coordinate method (GCM),^{1)–5)} cranked-Hartree-Fock-Bogoliubov plus local quasiparticle random phase approximation (CHFBLQRPA).⁶⁾ For highly excited states, (super)deformed states have been discussed on the basis of Hartree-Fock (-Bogoliubov+GCM)^{7)–10)} calculations, and their evolution to molecule-like cluster states is also studied by antisymmetrized molecular dynamics (AMD).^{11)–13)}

Among the *sd*-shell nuclei, ^{24}Mg has been the most studied in detail theoretically and experimentally. Furthermore, recent new experimental information obtained by the inelastic α scattering sheds new light on the highly excited states of ^{24}Mg . Namely, the triaxial deformation of the low-lying rotational bands has been discussed for a long time, which is associated with the presence of the $K^\pi = 2^+$ band built on the 2_2^+ state at 4.2 MeV.^{14), 15)} As an example of such theoretical efforts, one can refer to the pioneering work using the Hartree-Fock-Bogoliubov model.¹⁶⁾ Recent beyond mean-field model studies^{2)–5)} revealed that the triaxial deformation is essential for the $K^\pi = 2^+$ band. Although the properties of the positive-parity bands are theoretically and experimentally investigated in detail, those of the negative-parity bands are unclear. Experimentally, the band assignments of the negative-parity states are not well established. Since the triaxial deformation of the mean field plays an important role in the positive-parity states, it could also generate various bands in the negative-parity states.

When we turn to the highly excited states, we can expect a variety of cluster states. According to Ikeda's diagram,¹⁷⁾ a couple of threshold energies that decompose the system into two or three clusters such as $^{12}\text{C}+^{12}\text{C}$, $\alpha+^{20}\text{Ne}$ and $2\alpha+^{16}\text{O}$ are located at approximately 10 to 20 MeV in excitation energy. These threshold energies are higher than those of lighter $N = Z$ nuclei, and hence, cluster states of ^{24}Mg are expected to appear as highly excited states. Cluster model studies¹⁸⁾⁻²⁴⁾ have been devoted to revealing them, but to date, little is known and their existence has not been established well, except for the well-known $^{12}\text{C}+^{12}\text{C}$ molecular resonances that appear at the vicinity of the Coulomb barrier.²⁵⁾⁻²⁹⁾ Recently, motivated by the discovery of the 3α and 4α condensed states in ^{12}C ^{30),31)} and ^{16}O ,³²⁾ Itagaki et al.,³³⁾ Ichikawa et al.,³⁴⁾ von. Oertzen et al.³⁵⁾ and Kokalova et al.³⁶⁾ have suggested the $2\alpha+^{16}\text{O}$ cluster state in ^{24}Mg or $n\alpha$ condensation around the core nucleus. Their discussions based on the $n\alpha$ +core cluster models renewed interest in the $2\alpha+^{16}\text{O}$ clustering in ^{24}Mg . Indeed, recent experimental information on inelastic α scattering suggests the possible presence of cluster states in highly excited states.³⁷⁾ However, other cluster states such as $^{12}\text{C}+^{12}\text{C}$ and $\alpha+^{20}\text{Ne}$ should be theoretically treated at the same time, because their threshold energies are close to each other as mentioned above.

Thus, the spectrum of ^{24}Mg may contain a rich variety of nuclear many-body dynamics, triaxial deformed mean field of low-lying states and clusters of highly excited states. To illustrate it theoretically, the excitation spectrum covering a wide energy range should be investigated. Furthermore, since there coexist several different cluster threshold energies, the study without an *a priori* assumption of cluster structures is desirable. Therefore, in this series of papers, we will investigate the excitation spectrum of ^{24}Mg and study the structure changes in the wide energy region on the basis of AMD.^{13),38)-41)} Since AMD is capable of describing the excitation spectrum and various structures without any assumption on the symmetry of the wave function and cluster structure, it enables us to investigate how ^{24}Mg changes its structure as the excitation energy increases. In this first paper, we focus on the low-lying spectra of the positive- and negative-parity states and discuss their triaxial deformation. In our next paper, we will discuss the cluster states in highly excited states and cluster correlations in the low-lying states.

Our aim in this study is to examine the γ deformation in the low-lying negative-parity bands as well as that in the positive-parity bands. It is shown that the triaxial deformation is also important in the low-lying negative-parity states as well as in the $K^\pi = 2^+$ band. We have obtained four negative-parity bands, $K^\pi = 0^-, 1^-, 2^-$ and 3^- , which correspond to the experimentally suggested band assignment⁴²⁾ except for the $K^\pi = 2^-$ band. Among them, the $K^\pi = 0^-$ and 3^- bands are triaxial deformed and their spectra and $E2$ transitions are quite sensitive to γ deformation.

This paper is organized as follows. The AMD framework used in this study is explained in the next section. In §3, we discuss the energy surfaces and density distributions of the positive- and negative-parity states. By performing the angular momentum projection and GCM, the assignments of the positive- and negative-parity bands and effects of γ deformation are discussed. In the final section, we summarize this work.

§2. Theoretical framework

2.1. Hamiltonian and variational wave function

The Hamiltonian used in this study is given as

$$\hat{H} = \sum_i \hat{t}_i + \frac{1}{2} \sum_{ij} \hat{v}_{NN}(ij) + \frac{1}{2} \sum_{ij \in \mathcal{P}} \hat{v}_C(ij) - \hat{t}_{cm}. \quad (2.1)$$

As the effective interaction \hat{v}_{NN} , we have used the Gogny D1S interaction (D1S),⁴³⁾ and the Coulomb force \hat{v}_C is approximated with the sum of twelve Gaussians. To investigate the dependence of the results on the effective interaction, we have also used Gogny D1 interaction (D1).⁴⁴⁾ \hat{t}_{cm} takes care of the center-of-mass energy. Since the center-of-mass wave function is analytically separable from the internal wave function in the AMD framework, our calculation is free of the spurious center-of-mass motion.

The intrinsic wave function of the system with mass A is represented by a Slater determinant of single-particle wave packets,

$$\Phi_{int} = \mathcal{A}\{\varphi_1, \varphi_2, \dots, \varphi_A\}, \quad \varphi_i(\mathbf{r}) = \phi_i(\mathbf{r})\chi_i\xi_i, \quad (2.2)$$

where φ_i is the i th single particle wave packet consisting of the spatial ϕ_i , spin χ_i and isospin ξ_i parts. The local Gaussian located at \mathbf{Z}_i is employed as ϕ_i ,⁴⁰⁾

$$\begin{aligned} \phi_i(\mathbf{r}) &= \exp\left\{-\sum_{\sigma=x,y,z} \nu_\sigma \left(r_\sigma - \frac{Z_{i\sigma}}{\sqrt{\nu_\sigma}}\right)^2\right\}, \\ \chi_i &= \alpha_i\chi_\uparrow + \beta_i\chi_\downarrow, \quad |\alpha_i|^2 + |\beta_i|^2 = 1, \\ \xi_i &= \text{proton or neutron}. \end{aligned} \quad (2.3)$$

Here, \mathbf{Z}_i , α_i , β_i and ν_σ are the variational parameters. The use of the deformed Gaussian is essential for the discussion on triaxial deformation. When ν_x , ν_y and ν_z have different values (i.e., $\nu_x \neq \nu_y \neq \nu_z$), Eq. (2.3) describes a single particle motion in a triaxial deformed mean field.

The parity-projected wave function is employed as the variational wave function,

$$\Phi^\pi = \hat{P}^\pi \Phi_{int} = \frac{1 + \pi \hat{P}_x}{2} \Phi_{int}. \quad (2.4)$$

Variational parameters (\mathbf{Z}_i , α_i , β_i and ν_σ) are independently determined for each parity by the variational calculation with the β - γ constraint explained below.

2.2. Variation with β - γ constraint

We perform a variational calculation under constraint on the matter quadrupole deformation parameters β and γ . In the AMD framework, the β - γ constraint was first applied by Suhara and Kanada-En'yo.⁴⁵⁾ We basically follow their prescription, but modified the definitions of β and γ for convenience in the numerical calculation.

They are defined as

$$\langle x^2 \rangle = R_0^2 \left\{ 1 + \sqrt{\frac{5}{\pi}} \beta \cos \left(\gamma + \frac{2\pi}{3} \right) \right\}, \quad (2.5)$$

$$\langle y^2 \rangle = R_0^2 \left\{ 1 + \sqrt{\frac{5}{\pi}} \beta \cos \left(\gamma - \frac{2\pi}{3} \right) \right\}, \quad (2.6)$$

$$\langle z^2 \rangle = R_0^2 \left\{ 1 + \sqrt{\frac{5}{\pi}} \beta \cos \gamma \right\}, \quad (2.7)$$

$$R_0^2 = \frac{1}{3} (\langle x^2 \rangle + \langle y^2 \rangle + \langle z^2 \rangle), \quad (2.8)$$

where $\langle \hat{x}^2 \rangle$, $\langle \hat{y}^2 \rangle$ and $\langle \hat{z}^2 \rangle$ are the expectation values of those operators calculated from the intrinsic wave function, and the intrinsic coordinate is defined such that the relation $\langle \hat{x}^2 \rangle \leq \langle \hat{y}^2 \rangle \leq \langle \hat{z}^2 \rangle$ is satisfied. This definition is slightly different from the definitions by Bohr-Mottelson and Hill-Wheeler, that are customarily used, and it gives smaller values for β and γ than others definitions at the same $\langle \hat{x}^2 \rangle$, $\langle \hat{y}^2 \rangle$ and $\langle \hat{z}^2 \rangle$.

The parabolic potentials are added to the total energy to impose the β - γ constraint:

$$V_c = v_\beta (\langle \beta \rangle - \beta_0)^2 + v_\gamma (\langle \gamma \rangle - \gamma_0)^2, \quad (2.9)$$

$$\tilde{E} = \frac{\langle \Phi^\pi | \hat{H} | \Phi^\pi \rangle}{\langle \Phi^\pi | \Phi^\pi \rangle} + V_c. \quad (2.10)$$

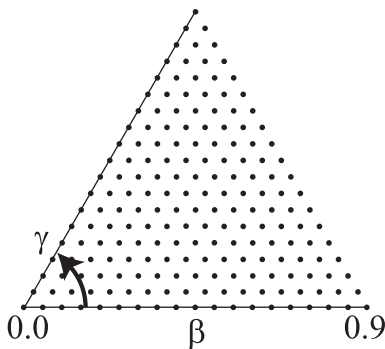


Fig. 1. Lattice in β - γ plane. Dots show the grid points where the variational calculation is performed.

Then, variational parameters of the intrinsic wave function are determined to minimize \tilde{E} for given β_0 and γ_0 by the frictional cooling method. The resultant wave function Φ^π has the minimum energy for a given set of (β_0, γ_0) and is called (denoted as) the parity-projected state ($\Phi^\pi(\beta_0, \gamma_0)$) in the following. In this study, the parity-projected states are calculated for discrete sets of (β, γ) on the triangular lattice in the β - γ plane, as shown in Fig. 1. The size of the lattice is 0.05 and the calculation is performed up to $\beta = 0.9$. v_β and v_γ

should be sufficiently larger than the curvature of the energy surface to obtain the exact minimum for a given (β_0, γ_0) as discussed in Ref. 46). However, the use of very large v_β and v_γ results in much longer calculation time and makes the energy convergence worse. Therefore, we have varied v_β and v_γ for every given value of (β_0, γ_0) during the variational calculation, so that the actual deformation of $\Phi^\pi(\beta_0, \gamma_0)$ is

close to (β_0, γ_0) . The deviations of $\Phi^\pi(\beta_0, \gamma_0)$ from (β_0, γ_0) are $\langle\beta\rangle - \beta_0 < 0.005$ and $\langle\beta\rangle - \beta_0 < 0.5^\circ$, and v_β and v_γ are typically varied within the range of $v_\beta = 200\text{--}4000$ MeV and $v_\gamma = 20\text{--}100$ MeV.

2.3. Angular momentum projection and GCM

After the variational calculation, we project out an eigenstate of the total angular momentum from the parity-projected states

$$\Phi_{MK}^{J\pi}(\beta_i, \gamma_i) = \hat{P}_{MK}^J \Phi^\pi(\beta_i, \gamma_i) / \sqrt{N_K^{J\pi}(\beta_i, \gamma_i)}, \quad (2.11)$$

$$\hat{P}_{MK}^J = \frac{2J+1}{8\pi^2} \int d\Omega D_{MK}^{J*}(\Omega) \hat{R}(\Omega), \quad (2.12)$$

$$N_K^{J\pi}(\beta_i, \gamma_i) = \langle \hat{P}_{MK}^{J\pi} \Phi^\pi(\beta_i, \gamma_i) | \hat{P}_{MK}^{J\pi} \Phi^\pi(\beta_i, \gamma_i) \rangle. \quad (2.13)$$

Here, \hat{P}_{MK}^J is the total angular momentum projector. The integrals are performed numerically over all the three Euler angles Ω 's as usual in the AMD framework, which is essential for the discussion of the degree of freedom of γ deformation. In the following, the state described by $\Phi_{MK}^{J\pi}(\beta_i, \gamma_i)$ is referred to as the K state (K is the projection of the angular momentum on the intrinsic z axis). The definition of the K state depends on the choice of the intrinsic coordinate. In this study, we defined the intrinsic z axis as the major axis. The choice of the intrinsic coordinate should not affect the result of the GCM calculation with K mixing. We have checked it and found that the differences in the eigenenergies are less than 100 keV in other choices of the intrinsic coordinate.

The calculation is completed by performing GCM. We superpose the K states $\Phi_{MK}^{J\pm}(\beta_i, \gamma_i)$, which have the same parity and angular momentum but have different K , deformation (β_i, γ_i) . Namely, the wave function of the system is formally expressed as

$$\Phi_\alpha^{J\pi} = \sum_i \sum_{K=-J}^J c_{Ki\alpha} \Phi_{MK}^{J\pi}(\beta_i, \gamma_i), \quad (2.14)$$

where the quantum numbers except the total angular momentum and the parity are represented by α . The coefficients $c_{Ki\alpha}$ are determined using the Hill-Wheeler equation

$$\sum_j \sum_{K'=-J}^J H_{KiK'j} c_{K'j} = E_\alpha \sum_j \sum_{K'=-J}^J N_{KiK'j} c_{K'j}, \quad (2.15)$$

$$H_{KiK'j} = \langle \Phi_{MK}^{J\pi}(\beta_i, \gamma_i) | \hat{H} | \Phi_{MK'}^{J\pi}(\beta_j, \gamma_j) \rangle, \quad (2.16)$$

$$N_{KiK'j} = \langle \Phi_{MK}^{J\pi}(\beta_i, \gamma_i) | \Phi_{MK'}^{J\pi}(\beta_j, \gamma_j) \rangle. \quad (2.17)$$

We call the solution of Eq. (2.15) triaxial GCM. The physical quantities discussed in the next section are basically calculated from the triaxial GCM wave function. To investigate the effects of γ deformation, we also performed the symmetry-restricted GCM calculation, in which the basis wave functions are limited to axial symmetric states ($\gamma = 0^\circ$ or 60°), which is called the axial GCM.

In the actual calculation, Eq. (2.15) is solved using the following procedure to maintain the numerical stability and make the analysis of the results transparent. First, we calculate the mixing between the different K states that have the same intrinsic deformation (β_i, γ_i) ,

$$\Phi_n^{J\pi}(\beta_i, \gamma_i) = \sum_{K=-J}^J f_{Kni} \Phi_{MK}^{J\pi}(\beta_i, \gamma_i), \quad (2.18)$$

$$\sum_{K=-J}^J H_{KK'} f_{K'ni} = e_n \sum_{K=-J}^J N_{KK'} f_{K'ni}. \quad (2.19)$$

$$H_{KK'} = \langle \Phi_{MK}^{J\pi}(\beta_i, \gamma_i) | \hat{H} | \Phi_{MK'}^{J\pi}(\beta_i, \gamma_i) \rangle, \quad (2.20)$$

$$N_{KK'} = \langle \Phi_{MK}^{J\pi}(\beta_i, \gamma_i) | \Phi_{MK'}^{J\pi}(\beta_i, \gamma_i) \rangle. \quad (2.21)$$

The generalized eigenvalue problem Eq. (2.19) is solved by the double diagonalization of $N_{KK'}$ and $H_{KK'}$. The states that have a very small eigenvalue of the norm-kernel $N_{KK'}$ should be omitted for numerical stability. The cutoff of the norm eigenvalue can be deduced from the number of digits of the matrix elements of H and N calculated accurately. In this study, we put the cutoff of the smallest norm eigenvalue as 10^{-3} . We call this calculation K -mixing and the solutions of Eq. (2.19) are called K -mixed states.

Then, we superpose all the K -mixed states with different deformations (β_i, γ_i) to take care of the fluctuation of the wave function in the β - γ plane:

$$\Phi_\alpha^{J\pi} = \sum_{i,n} g_{nia} \Phi_n^{J\pi}(\beta_i, \gamma_i), \quad (2.22)$$

$$\sum_{n'j} H_{nin'j} g_{n'j\alpha} = E_\alpha \sum_{n'j} N_{nin'j} g_{n'j\alpha}, \quad (2.23)$$

$$H_{nin'j} = \langle \Phi_n^{J\pi}(\beta_i, \gamma_i) | \hat{H} | \Phi_{n'}^{J\pi}(\beta_j, \gamma_j) \rangle, \quad (2.24)$$

$$N_{nin'j} = \langle \Phi_n^{J\pi}(\beta_i, \gamma_i) | \Phi_{n'}^{J\pi}(\beta_j, \gamma_j) \rangle. \quad (2.25)$$

By solving Eq. (2.23), we obtain the GCM results. Combining Eqs. (2.14), (2.18) and (2.22), one finds the relations:

$$\Phi_\alpha^{J\pi} = \sum_i \sum_{K=-J}^J c_{Ki\alpha} \Phi_{MK}^{J\pi}(\beta_i, \gamma_i) \quad (2.26)$$

$$= \sum_i \sum_{K=-J}^J \left(\sum_n f_{Kni} g_{ni\alpha} \right) \Phi_n^{J\pi}(\beta_i, \gamma_i), \quad (2.27)$$

$$c_{Ki\alpha} = \sum_n f_{Kni} g_{ni\alpha}. \quad (2.28)$$

To discuss the fluctuation of the triaxial GCM wave function in the β - γ plane, it is convenient to use the overlap between the triaxial GCM wave function and the K -mixed states,

$$O_{n\alpha}^{J\pi}(\beta_i, \gamma_i) = |\langle \Phi_n^{J\pi}(\beta_i, \gamma_i) | \Phi_\alpha^{J\pi} \rangle|^2. \quad (2.29)$$

The behavior of $O_{n\alpha}^{J\pi}(\beta_i, \gamma_i)$ in the β - γ plane is discussed in the next section.

§3. Results and discussion

3.1. Energy surfaces and the triaxial deformation

Figure 2 shows the energy surfaces calculated from the parity-projected states obtained by using the D1S parameter set,

$$E^\pi(\beta, \gamma) = \frac{\langle \Phi^\pi(\beta, \gamma) | \hat{H} | \Phi^\pi(\beta, \gamma) \rangle}{\langle \Phi^\pi(\beta, \gamma) | \Phi^\pi(\beta, \gamma) \rangle}. \quad (3.1)$$

The positive-parity states have a prolate-deformed minimum at $(\beta, \gamma) = (0.4, 0^\circ)$, and a saddle point with oblate deformation, $(\beta, \gamma) = (0.18, 60^\circ)$. As mentioned in other studies,^{2),3)} this oblate-deformed saddle point imitates the second minimum on the energy curve if we restrict the calculation to be axial symmetric. The D1 parameter set gives qualitatively the same result in both parity states, but D1 gives a smaller binding energy than D1S by about 5 MeV in the entire region of the energy surface, and makes the energy surface very slightly softer against γ deformation. Since the dependence of the GCM results on the choice of Gogny parameter sets is minor except for the total binding energy, we mainly discuss the results obtained with the D1S parameter sets, and the differences between D1S and D1 are explained in the following subsections.

The behavior of the surface is similar to and qualitatively consistent with other triaxial calculations.^{2),3)} Rodríguez and Egido³⁾ performed the particle-number-projected triaxial Hartree-Fock-Bogoliubov calculation that use the same effective interaction as our calculation. Compared with their result, there are some quantitative deviations. For example, the β deformation of the minimum and the slope of the surface are slightly different. These deviations come from the difference between the definitions of β and γ and from the treatment of the pairing correlation, which is not explicitly implemented in our model. Differently from Rodríguez and Egido's calculation, we perform the parity projection and do not assume the time-reversal

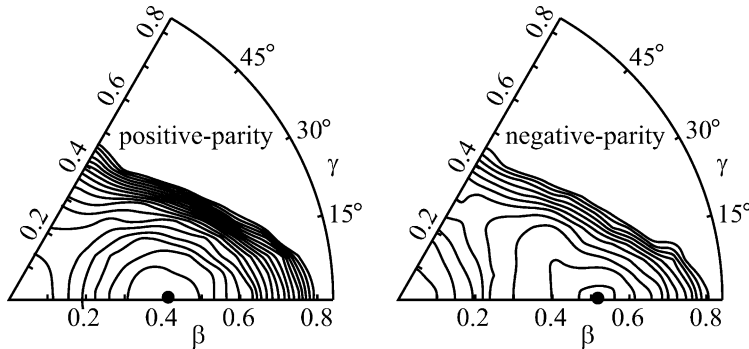


Fig. 2. Energy surfaces in β - γ plane for positive- and negative-parity states obtained with the D1S parameter set. Dots show the energy minima and the contour shows the increase of energy for every 1 MeV.

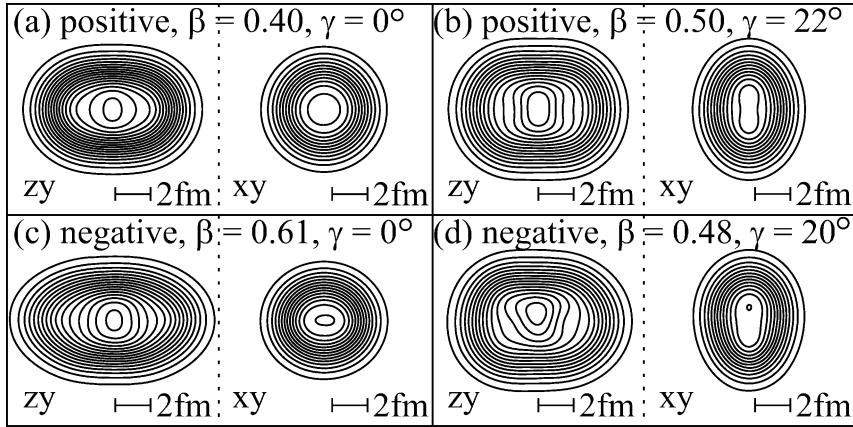


Fig. 3. Intrinsic matter density distributions obtained with the D1S parameter set. (a) and (c) show the axial symmetric states that respectively dominate the ground band and $K^\pi = 1^-, 2^-$ bands after the GCM calculation. (b) and (d) show the triaxial states that respectively dominate the $K^\pi = 2^+$ and $K^\pi = 0^-, 3^-$ bands.

symmetry. They also lead to a quantitative difference in the results.

The intrinsic density distributions of the minimum and triaxial deformed states are respectively shown in Figs. 3(a) and (b). The latter becomes the dominant component of the $K^\pi = 2^+$ band after the triaxial GCM calculation. The states show almost parity-symmetric axial or triaxial deformation. We see the absence of the clustering in the states such as $2\alpha + {}^{16}\text{O}$ and ${}^{12}\text{C} + {}^{12}\text{C}$. The absence of the clusterlike structure is common to all the calculated parity-projected states in this work. This may indicate that the low-lying spectrum of ${}^{24}\text{Mg}$ is dominated by the mean field and its dynamics. However, it must be emphasized that it does not necessarily indicate the absence of the cluster structure in the excited states nor the absence of the clustering correlation in the low-lying states. This point will be the focus of our discussion in the next work.

The parity projection before variation makes it possible to investigate the deformation of the negative-parity states. The negative-parity states also have a prolate deformed minimum at $(\beta, \gamma) = (0.51, 0^\circ)$ and an oblate deformed saddle at $(\beta, \gamma) = (0.27, 60^\circ)$. They are connected along the valley of the energy surface. This suggests the importance of the degree of freedom of γ deformation in the negative-parity states as well as in the positive-parity states. Compared with the positive-parity states, these states have a larger β deformation. This is due to the nucleon excitations from the p - to sd -shell. The intrinsic density distributions of the minimum and triaxial deformed states are respectively shown in Figs. 3(c) and (d). The latter becomes the dominant component of the $K^\pi = 0^-$ and 3^- bands after the GCM calculation. Although the axial symmetric state (Fig. 3(c)) shows an almost parity-symmetric density distribution, the triaxial state (Fig. 3(d)) shows the asymmetry in the xy plane. Again, we recognize no sign of prominent clustering in any calculated states.

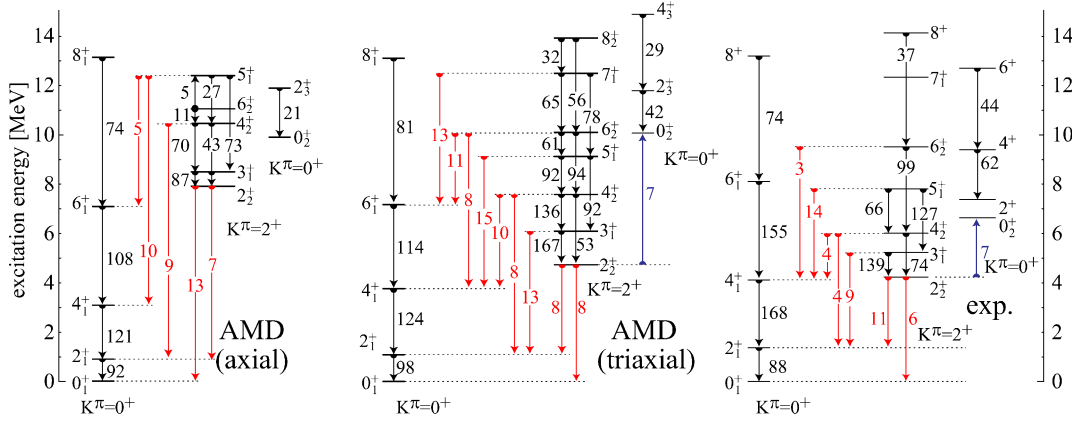


Fig. 4. (color online) Calculated (D1S) and observed partial level scheme and $B(E2)$ of ^{24}Mg for the positive-parity states. Left: axial GCM, middle: triaxial GCM and right: experiments.^{(47)–(51)}

3.2. Positive-parity bands

By performing the angular momentum projection and triaxial and axial GCMs, we calculated the excitation spectrum. The triaxial GCM generates three rotational bands including the ground band. Figure 4 shows a comparison of the calculated and observed^{(47)–(51)} positive-parity spectra. The band assignments of the GCM results are based on the calculated $B(E2)$ strength.

3.2.1. $J^\pi = 0^+$ and 2^+ states by triaxial GCM

To understand the structure of each state obtained by the triaxial GCM calculation, we first discuss the energy surface and wave functions of the $J^\pi = 0^+$ and 2^+ states. In the case of the $J^\pi = 0^+$ state, it does not have K mixing by definition, and the energy surface of the $K^\pi = 0^+$ states is shown by the contour lines in Fig. 5(a) (Fig. 5(b) also shows the same contour line). Owing to the angular momentum projection, a triaxial state at $(\beta, \gamma) = (0.49, 13^\circ)$ becomes the lowest energy state. This state energy is decreased by 7.3 MeV after the angular momentum projection, and it is 1 MeV lower than the prolate deformed saddle point at $\beta = 0.5$. The triaxial GCM generates 0_1^+ and 0_2^+ states on this energy surface. The binding energy of the ground state is 198.55 MeV and it overestimates the observed value (198.26 MeV) by 0.3 MeV. The calculated excitation energy of the 0_2^+ state is 10.1 MeV, while the observed value is 6.4 MeV. In the case of the D1 parameter set, the total binding energy is underestimated (192.98 MeV), but the excitation energy of the 0_2^+ state is slightly better (9.7 MeV).

The overlaps of these 0^+ states with the $K^\pi = 0^+$ wave function on the energy surface are shown by the color plots in Figs. 5(a) and (b). The overlaps show that the ground state has a broad fluctuation in the β - γ plane and it is centered at the minimum of the energy surface (Fig. 5(a)). This broad distribution is partly due to the softness of the energy surface against β and γ deformations. Another reason is the unorthogonality of the $K^\pi = 0^+$ wave functions on the energy surface. For example, the wave function at the triaxial minimum and that at the saddle point

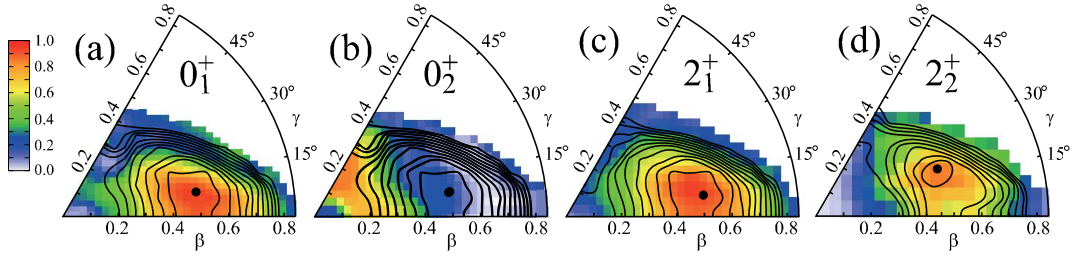


Fig. 5. (color online) Energy surfaces and overlaps of $J^\pi = 0^+$ and 2^+ states calculated with the D1S parameter set. The contours show the energies of the K -mixed states with an interval of 1 MeV, and dots show the minima position. The color plots show the overlaps of each state with K -mixed states.

on the $\gamma = 0^\circ$ line have a large overlap that amounts to about 90%. Therefore, both wave functions naturally have a large overlap with the GCM wave function. In contrast to the ground state, the 0_2^+ state has an overlap concentrated on the oblate side with a smaller β . As we will see later, the $K^\pi = 0_1^+$ and 0_2^+ bands are built on these 0^+ states.

In the case of the $J^\pi = 2^+$ states, there literary exist five K states with $K^\pi = -2^+-2^+$. Among them, three K -states ($K^+ = 0^+$ and $\pm 2^+$) have a large norm after the angular momentum projection. By the K -mixing, we obtain two independent K -mixed states. The K -mixed state with the lowest energy is dominated by the $K^\pi = 0^+$ wave function, while the second lowest K -mixed state is dominated by the $K^\pi = \pm 2^+$ wave functions. Their energy surfaces are respectively shown in Figs. 5(c) and (d). The behavior of the energy surface of the lowest K -mixed states (Fig. 5(c)) is similar to that of the $J^\pi = 0^+$ states (Fig. 5(a)). It has a triaxial deformed minimum at the same deformation with the $J^\pi = 0^+$ states and is soft against β and γ deformations. On the other hand, the second lowest K -mixed state shows a different behavior. It has a pronounced triaxial minimum at $(\beta, \gamma) = (0.49, 18^\circ)$. By performing the triaxial GCM, we obtain the 2_1^+ , 2_2^+ and 2_3^+ states at 1.1, 4.7 and 11.8 MeV, respectively. The 2_1^+ and 2_3^+ states are dominated by the lowest K -mixed states (therefore, $K^\pi = 0^+$ states), and classified into the $K^\pi = 0_1^+$ and 0_2^+ bands, as we will see below. The 2_2^+ state is dominated by the second lowest K -mixed state ($K^\pi = \pm 2^+$), and the $K = 2^+$ band is built on this state.

The overlap between the 2_1^+ state and the lowest K -mixed state is shown in Fig. 5(c) by a color plot. It shows a broad fluctuation in the β - γ plane centered at the minimum of the energy surface and quite a similar behavior to the ground state. It is also noted that the overlap of the 2_3^+ state is similar to that of the 0_2^+ state, although it is not shown in the figure. The overlaps of these states are consistent with the band assignment. Since the fluctuations in the β - γ plane are similar to each other, the $B(E2)$ between 0_1^+ and 2_1^+ and that between 0_2^+ and 2_3^+ are large. Different from other 2^+ states, the 2_2^+ state is dominated by the second lowest K -mixed state. Figure 5(d) shows the overlap between the 2_2^+ state and the second lowest K -mixed state. The overlap is centered at the minimum of the energy surface that has a larger γ value than the 2_1^+ and 2_3^+ states. This suggests the importance of

the γ deformation for the 2_2^+ state, which will become clearer by comparing it with the axial GCM result.

3.2.2. Band assignment and triaxial deformation

The characteristics of 2^+ states discussed above are common to other natural parity states such as the 4^+ and 6^+ states. Namely, we always obtain two K -mixed states. The lowest and second lowest K -mixed states are respectively dominated by the $K^\pi = 0^+$ and $K^\pi = \pm 2^+$ states. The former constitutes the $K^\pi = 0_1^+$ and 0_2^+ band member states, and the latter constitutes the $K^\pi = 2^+$ band. In the case of the unnatural parity states, we always obtain one K -mixed state dominated by the $K^\pi = \pm 2^+$ states, and they are assigned to the $K^\pi = 2^+$ band.

The calculated and observed ground band spectra show rather good agreement including the intraband $E2$ transitions. However, there are slight differences between the spectra of the high-spin states. Although the calculated ground band is a rotational spectrum, the observed energy spacing between 6_1^+ and 8_1^+ shows a deviation from the rotor. To reproduce this deviation, we may need to perform variational calculation after angular momentum projection. Since there are no qualitative differences between the axial and triaxial calculations, we can conclude that γ deformation is not essential to the ground band.

In contrast to those of the ground band, the spectra of the $K^\pi = 2^+$ band obtained by axial and triaxial GCM are quite different. The axial GCM gives about 4 MeV higher excitation energy of the 2_2^+ state than the triaxial GCM and observation. Furthermore, it gives an irregular excitation energy of the 5_1^+ state and much smaller intraband $E2$ transitions. Apparently, the axial GCM fails to describe the observed $K^\pi = 2^+$ band, while the triaxial GCM is compatible with the observation. Thus, the degree of freedom of γ deformation is essential to describe the $K^\pi = 2^+$ band. This point was also emphasized in other triaxial calculations.^{2),3)} It is also noted that the D1 parameter set gives a slightly smaller excitation energy of the 2_2^+ state by about 0.2 MeV.

Experimentally, the $K^\pi = 0_2^+$ band is built on the 0_2^+ state at 6.4 MeV. Both axial and triaxial calculations with the D1S and D1 parameter sets overestimate the excitation energy of the 0_2^+ state by about 4 MeV. The HFB+GCM calculation using the same effective interaction also overestimates the energy of this state. This discrepancy may be attributed to either (1) the property of Gogny force or (2) the insufficiency of the model space to describe this band. For example, as we have explained in the previous section, no clusterlike configurations are included in the present calculation or HFB+GCM calculations. The nature of this $K^\pi = 0_2^+$ band will be investigated in detail in our next work.

3.3. Negative-parity bands

By the triaxial GCM with the D1S parameter set, we obtain four rotational bands, which we call $K^\pi = 0^-, 1^-, 2^-$ and 3^- as shown in Fig. 6. The $K^\pi = 1^-$ and 2^- bands are prolate deformed, while the $K^\pi = 0^-$ and 3^- bands are triaxial deformed. The same as that in the case of the positive-parity bands, this band assignment is based on the strength of the $B(E2)$. The D1 parameter set gives

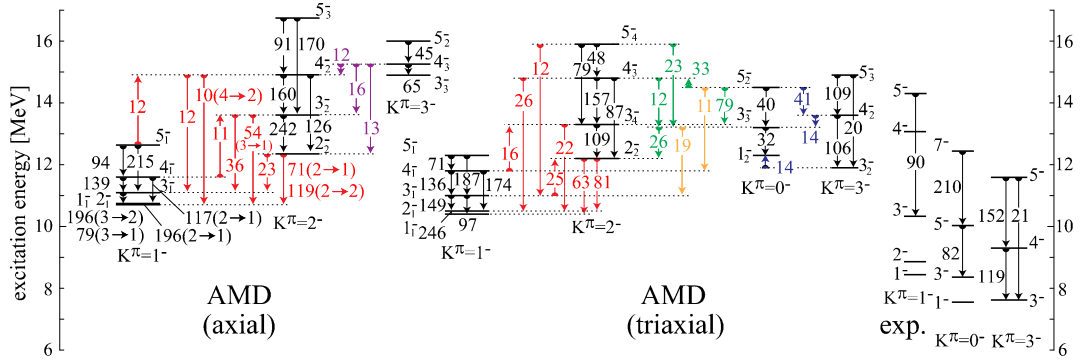


Fig. 6. (color online) Same as Fig. 4, but for the negative-parity states. Experimental data are cited from Ref. 42).

slightly higher excitation energies for all the negative-parity states by about 0.5 MeV, but the band structure is common to the D1S parameter set discussed below.

3.3.1. $J^\pi = 1^-, 2^-$ and 3^- states by triaxial GCM

The structures of the negative-parity bands are rather complicated, and hence, we first discuss the structure of the $J^\pi = 1^-, 2^-$ and 3^- states. There are three K states with $K = 0$ and ± 1 for $J^\pi = 1^-$, and after the K -mixing, we obtain two K -mixed states. The lowest energy state is dominated by the $K = \pm 1$ states and has a prolate minimum at $(\beta, \gamma) = (0.6, 0^\circ)$ (contour line of Fig. 7(a)). The 1_1^- state at 10.5 MeV is distributed around this minimum and it is the band head of the $K^\pi = 1^-$ band. The second lowest K -mixed state is dominated by the $K = 0$ states and has a triaxial minimum at $(\beta, \gamma) = (0.5, 25^\circ)$ (contour in Fig. 7(b)). The 1_2^- state at 12.3 MeV predominantly constitutes of this triaxial state, which is confirmed in Fig. 7(b).

In the case of $J^\pi = 2^-$ states, we obtain four K states with $K = \pm 1$ and ± 2 . These states are strongly mixed with each other by the K -mixing, and we obtain two K -mixed states. Both are prolate deformed and have minima around $(\beta, \gamma) = (0.6, 0^\circ)$ (Fig. 7(c) shows the second lowest state). The lowest state is assigned as the member state of the $K^\pi = 1^-$ band, while the second lowest state

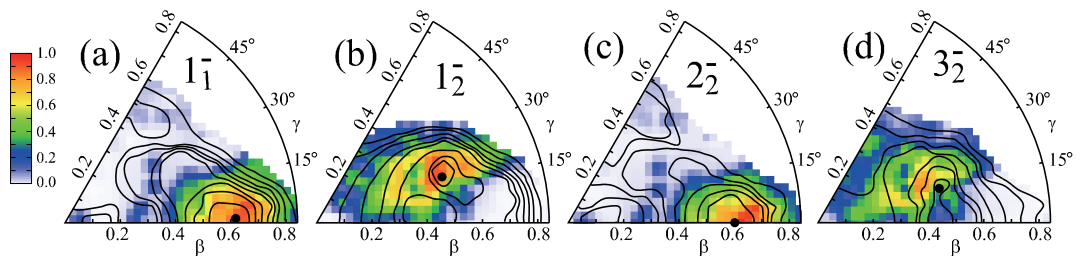


Fig. 7. (color online) Energy surfaces and overlaps of $J^\pi = 1^-, 2^-$ and 3^- states calculated with the D1S parameter set. Contour show the energies of the K -mixed states with interval of 1 MeV, and dots show the minima position. Color plot shows the overlap of each state with K -mixed states.

is assigned as the band head of the $K^\pi = 2^-$ band on the basis of the strength of the $E2$ transition probability. Owing to the strong mixing between the $K^\pi = \pm 1$ and ± 2 states and strong deformation, both $2_1^- \rightarrow 1_1^-$ ($K^\pi = 1^-$ intraband) and $2_2^- \rightarrow 1_1^-$ ($K^\pi = 2^- \rightarrow K^\pi = 1^-$ interband) $E2$ transitions have large probabilities.

For the $J^\pi = 3^-$ states, we obtain the $K = 0^-, \pm 1^-, \pm 2^-, \pm 3^-$ states. The $K^\pi = \pm 1^-$ and $\pm 2^-$ states have prolate minima and the $K^\pi = 0^-$ and $\pm 3^-$ states have triaxial minima. By the K -mixing, we obtain four independent states. The $K^\pi = \pm 1^-$ and $\pm 2^-$ states are strongly mixed with each other as they were in the $J^\pi = 2^-$ states, and they constitute the first and fourth lowest K -mixed states. They predominate the 3_1^- and 3_4^- states that are assigned to the $K^\pi = 1^-$ and 2^- bands, respectively. The $K = 0^-$ and $\pm 3^-$ states are also strongly mixed with each other by the K mixing and constitute the second and third lowest K -mixed states. These triaxial deformed states constitute the 3_2^- and 3_3^- states that are the member states of the $k^\pi = 3^-$ and 0^- bands.

3.3.2. Negative-parity bands

The natural parity states that have larger angular momentum than $J = 3^-$ are similar to the $J = 3^-$ states. Namely, there are the $K^\pi = 0^-, \pm 1^-, \pm 2^-$ and $\pm 3^-$ states. The $K^\pi = \pm 1^-$ and $\pm 2^-$ states are prolate deformed and strongly mixed by the K -mixing. The states dominated by them are assigned to the $K^\pi = 1^-$ and 2^- bands. The $K^\pi = 0^-$ and $\pm 3^-$ states are triaxial deformed and mixed with each other. They constitute the $K^\pi = 0^-$ and 3^- bands. Thus, we obtain four negative-parity bands, i.e., the $K^\pi = 0^-, 1^-, 2^-$ and 3^- bands. Two of them are prolate deformed and the other two are triaxial deformed. Owing to the strong K mixing, the interband transition between the $K^\pi = 1^-$ and 2^- bands and the $K^\pi = 0^-$ and 3^- bands are rather strong. There is also mixing between the $K^\pi = 0^-$ and 2^- states in the $J^\pi = 5^-$ states, and hence, the interband $E2$ transitions between the $K^\pi = 0^-$ and 2^- bands are strong.

The experimental band assignment of the negative-parity states is not well established. In the following we compare our result with the assignment by Fifield et al.,⁴²⁾ which suggests the $K^\pi = 3^-, 0^-$ and 1^- bands starting from 7.62, 7.55 and 8.44 MeV, respectively. The agreement between the observation and the present calculation is not as good as that in the positive-parity states. Although the observed negative-parity bands start from approximately 8 MeV, the calculated bands start from 10 to 12 MeV. Nevertheless, the calculated $K^\pi = 1^-, 0^-$ and 3^- bands may correspond to the observed bands from their in-band $E2$ transitions. By comparing axial GCM and triaxial GCM, one finds that the γ deformation is important for describing the $K^\pi = 0^-$ and 3^- bands. The $K^\pi = 0^-$ band is missing in the axial GCM calculation and the energy of the $K^\pi = 3^-$ band is markedly reduced by the triaxial GCM. On the other hand, the γ deformation is less important for the $K^\pi = 1^-$ and 2^- bands. Compared with the observation, the energies of the $K^\pi = 0^-$ and 3^- bands are overestimated by about 4 MeV. In addition to the $K^\pi = 1^-$ band, as the axial deformed band, the calculation predicts the $K^\pi = 2^-$ band that is not experimentally established yet. However, the cluster model calculation also predicted this band and it is noted that the candidates of the member states of this band were

suggested in Ref 21).

§4. Summary

In summary, we have investigated the low-lying spectrum of ^{24}Mg using AMD and focused on γ deformation. We have obtained seven rotational bands. The assignment of the three positive-parity bands is experimentally well established and our results show a good agreement except for the $K^\pi = 0_2^+$ band. Among them, the importance of γ deformation for the $K^\pi = 2^+$ band is confirmed, while the other two bands are insensitive to γ deformation. In the case of the negative-parity band, the experimental band assignment is not established yet. We have obtained four negative parity rotational bands, i.e., $K^\pi = 0^-, 1^-, 2^-$ and 3^- . Except for the $K^\pi = 2^-$ band, our results qualitatively agree with the assignment suggested in Ref. 42), although the excitation energies are overestimated by about 5 MeV. It is found that γ deformation also plays an important role in the negative-parity states. The properties of the $K^\pi = 3^-$ and 0^- bands are quite sensitive to the γ deformation.

The states discussed in this paper do not show a prominent cluster structure. Therefore, clustering is less important for the low-lying states, and the triaxial deformed mean field appears more essential. However, note that the excitation energies of several bands are overestimated in this study. For example, the energy of the $K^\pi = 0_2^+$ band is overestimated by 4 MeV, while the two other positive-parity bands are well reproduced. Clusterlike correlation may be important for describing the $K^\pi = 0_2^+$ band. In our next paper, we will discuss the clusterlike correlation in the low-lying states and prominent clustering of highly excited states.

References

- 1) R. R. Rodriguez-Guzman, J. L. Egido and L. M. Robledo, *Eur. Phys. J. A* **17** (2003), 37.
- 2) M. Bender and P.-H. Heenen, *Phys. Rev. C* **78** (2008), 024309.
- 3) T. R. Rodriguez and J. L. Egido, *Phys. Rev. C* **81** (2010), 064323.
- 4) J. M. Yao, J. Meng, P. Ring and D. Vretenar, *Phys. Rev. C* **81** (2010), 044311.
- 5) J. M. Yao, H. Mei, H. Chen, J. Meng, P. Ring and D. Vretenar, *Phys. Rev. C* **83** (2011), 014308.
- 6) N. Hinohara and Y. Kanada-En'yo, *Phys. Rev. C* **83** (2011), 014321.
- 7) R. R. Rodriguez-Guzman, J. L. Egido and L. M. Robledo, *Phys. Rev. C* **62** (2000), 054308.
- 8) T. Inakura, S. Mizutori, M. Yamagami and K. Matsuyanagi, *Nucl. Phys. A* **710** (2002), 261.
- 9) M. Bender, F. Flocarda and P.-H. Heenen, *Phys. Rev. C* **68** (2003), 044321.
- 10) T. Inakura, H. Imagawa, Y. Hashimoto, S. Mizutori, M. Yamagami and K. Matsuyanagi, *Nucl. Phys. A* **768** (2006), 61.
- 11) M. Kimura and H. Horiuchi, *Phys. Rev. C* **69** (2004), 051304.
- 12) Y. Kanada-En'yo and M. Kimura, *Phys. Rev. C* **72** (2005), 064322.
- 13) Y. Taniguchi, M. Kimura, Y. Kanada-En'yo and H. Horiuchi, *Phys. Rev. C* **76** (2007), 044317.
- 14) R. Batchelor, A. J. Ferguson, H. E. Gove and A. E. Litherland, *Nucl. Phys.* **16** (1960), 38.
- 15) A. Cohen and J. Cookson, *Nucl. Phys.* **29** (1962), 604.
- 16) M. Girod and B. Grammaticos, *Phys. Rev. C* **27** (1983), 2317.
- 17) K. Ikeda, N. Tagikawa and H. Horiuchi, *Prog. Theor. Phys. Suppl. Extra Number* (1968), 464.
- 18) T. Matsuse, Y. Kondō and Y. Abe, *Prog. Theor. Phys.* **59** (1978), 1009.

- 19) K. Katō and H. Bando, Prog. Theor. Phys. **62** (1979), 644.
- 20) Y. Kondō, Y. Abe and T. Matsuse, Phys. Rev. C **19** (1979), 1356.
- 21) M. Ohkubo, K. Katō and H. Tanaka, Prog. Theor. Phys. **67** (1982), 207.
- 22) D. Baye and P. Descouvemont, Nucl. Phys. A **419** (1984), 397.
- 23) P. Descouvemont and D. Baye, Nucl. Phys. A **475** (1987), 219.
- 24) P. Descouvemont, Nucl. Phys. A **709** (2002), 275.
- 25) E. Almqvist, D. A. Bromely and J. A. Kuehner, Phys. Rev. Lett. **4** (1960), 515.
- 26) M. Mazarakis and W. E. Stephens, Phys. Rev. C **7** (1973), 1280.
- 27) E. R. Cosman et al., Phys. Rev. Lett. **35** (1975), 265.
- 28) K. A. Erb et al., Phys. Rev. Lett. **37** (1976), 670.
- 29) H. T. Fortune et al., Phys. Rev. C **15** (1977), 439.
- 30) A. Tohsaki, H. Horiuchi, P. Schuck and G. Ropke, Phys. Rev. Lett. **87** (2001), 192501.
- 31) Y. Funaki, A. Tohsaki, H. Horiuchi, P. Schuck and G. Ropke, Phys. Rev. C **67** (2003), 051306.
- 32) Y. Funaki, T. Yamada, H. Horiuchi, G. Ropke, P. Schuck and A. Tohsaki, Phys. Rev. Lett. **101** (2008), 082502.
- 33) N. Itagaki, M. Kimura, C. Kurokawa, M. Ito and W. von Oertzen, Phys. Rev. C **75** (2007), 037303.
- 34) T. Ichikawa, N. Itagaki, T. Kawabata, Tz. Kokalova and W. von Oertzen, Phys. Rev. C **83** (2011), 061301.
- 35) W. von Oertzen, Eur. Phys. J. A **29** (2006), 133.
- 36) Tz. Kokalova et al., Eur. Phys. J. A **23** (2005), 19.
- 37) T. Kawabata et al., AIP Conf. Proc. **1355** (2011), 194.
- 38) Y. Kanada-En'yo, H. Horiuchi and A. Ono, Phys. Rev. C **52** (1995), 628.
- 39) Y. Kanada-En'yo, H. Horiuchi and A. Doté, Phys. Rev. C **60** (1999), 064304.
- 40) M. Kimura, Phys. Rev. C **69** (2004), 044319.
- 41) M. Kimura and H. Horiuchi, Nucl. Phys. A **767** (2006), 58.
- 42) L. K. Fifield et al., Nucl. Phys. A **322** (1979), 1.
- 43) J. Dechage and D. Gogny, Phys. Rev. C **21** (1980), 1568.
- 44) J. P. Blaizot and D. Gogny, Nucl. Phys. A **284** (1977), 429.
- 45) T. Suhara and Y. Kanada-En'yo, Prog. Theor. Phys. **123** (2010), 303.
- 46) P. Ring and P. Schuck, *The Nuclear Many-Body Problem* (Springer-Verlag, New York, 1980), Chap 7.6.
- 47) M. A. Meyer, J. P. L. Reinecke and D. Reitmann, Nucl. Phys. A **185** (1972), 625.
- 48) D. Branford, A. C. McGough and I. F. Wright, Nucl. Phys. A **241** (1975), 349.
- 49) J. D. Garrett, H. T. Fortune, R. Middleton and W. Scholz, Phys. Rev. C **18** (1978), 2032.
- 50) B. Zwieglinski, G. M. Crawley, H. Nann and J. A. Nolen, Phys. Rev. C **17** (1978), 872.
- 51) L. K. Fifield, M. J. Hurst, T. J. M. Symons, F. Watt, C. H. Zimmerman and K. W. Allen, Nucl. Phys. A **309** (1978), 77.